

# Investigation of Freeze Linings in Copper-Containing Slag Systems: Part II. Mechanism of the Deposit Stabilization

ATA FALLAH-MEHRJARDI, PETER C. HAYES, and EVGUENI JAK

A major industrial problem in high-temperature liquid reaction systems is the attack of furnace components by chemically aggressive molten reactants. Freeze-lining technologies involving the deliberate formation of controlled frozen deposits are increasingly being applied to extend the range of liquid bath compositions and process temperatures that can be used; this has resulted in significant increases in process performance and productivity. It has been widely assumed that the interface between the stationary frozen layer and the agitated molten bath at steady state consists of the primary phase, which stays in contact with the bulk liquid at the liquidus temperature,  $T_{\text{liquidus}}$ . It has been shown in the current laboratory-based studies through the use of a cold finger technique that, at steady state and in selected ranges of process conditions and bath compositions, the phase assemblage present at the deposit/liquid interface is not that of the primary phase alone. The microstructural observations clearly demonstrate that the temperature of the deposit/liquid bath interface,  $T_f$ , can be lower than the liquidus temperature of the bulk liquid,  $T_{\text{liquidus}}$ . These observations point to a significant change in the mechanism and behavior of the systems. To explain this phenomenon, it is proposed that the steady-state thickness of freeze linings is not the result of equilibrium freezing but rather represents a state of dynamic equilibrium that is critically dependent on the relative rates of crystallization, mass, and heat transfer processes, occurring close to and at the deposit interface. The mechanisms taking place in the boundary liquid layer involve both partial crystallization/remelting and continuous removal of solids. This finding has important implications for the design of the high-temperature industrial reactors and selection of ranges of melt chemistries and conditions that can be used. This finding means that temperatures below the liquidus can be selected for some processes, resulting potentially in significant savings of energy and increases in throughput of pyrometallurgical reactors. The findings are generic and are not limited to the specific chemical systems reported in the article.

DOI: 10.1007/s11663-013-9807-y

© The Minerals, Metals & Materials Society and ASM International 2013

## I. INTRODUCTION

TO date, the designs of freeze-lining for pyrometallurgical furnaces have been based almost exclusively on heat-transfer considerations.<sup>[1–9]</sup> There is increasing evidence, however, to show that optimum practice should also take into account the effects of bath chemistry. In part I of this series,<sup>[10]</sup> a range of microstructures in freeze-lining deposits formed from copper-containing slags was described. The freeze-lining deposits in general have been found to consist of several different layers. Starting from the cold wall, these layers consist of 1) glass, 2) glass with microcrystalline precipitates, 3) multiphase subliquidus material containing solid delafossite and cuprite and high-silica liquid that is separated from the bulk liquid (closed crystalline layer), and 4) a complex phase assemblage containing

delafossite and cuprite crystals and a high-silica liquid phase that is connected to the bulk liquid (open crystalline layer). A dense layer of primary phase crystals of bulk bath—the fifth layer called the primary phase sealing layer—has not been observed in any of the steady-state deposits in the current study.<sup>[10]</sup> This is very different from the anticipated structure of stationary deposit-bath interface at steady-state conditions—it was expected that the deposit interface would consist solely of the primary phase crystals, delafossite.

The reasoning behind the expectation of the presence of the primary phase sealing layer is that at steady-state conditions, the crystal phases are already present at the stationary deposit so there is no nucleation barrier to overcome, and crystallization on the outer surface of the interface with the bath would take place due to continuous heat removal through the stationary deposit as well as continuous supply of fresh chemicals from the bulk bath to the interface by relatively fast mass transfer through the agitated layers of liquid until equilibrium is reached at liquidus temperature of the bulk bath ( $T_{\text{liquidus}}$ ).

These observations reported in the Part I of this series indicate the need to further investigate the mechanisms of freeze-lining formation and the effects of chemically

---

ATA FALLAH-MEHRJARDI, Ph.D. Student, PETER C. HAYES, Xstrata Professor of Metallurgical Engineering, and EVGUENI JAK, Professor, are with the PYROSEARCH, School of Chemical Engineering, The University of Queensland, Brisbane, Australia. Contact e-mail: a.fallahmehrjardi@uq.edu.au

Manuscript submitted July 27, 2012.

Article published online February 16, 2013.

relevant parameters on the microstructure, stability, thickness, and overall heat transfer of freeze lining particularly at steady-state conditions.

## II. EXPERIMENTAL METHODOLOGY

The details of the experimental methods and techniques used in the current study have been described in part I of this series.<sup>[10]</sup> Briefly, the current laboratory studies have been undertaken using an air-cooled probe, or so-called “cold finger” technique. The probe is immersed in a molten slag bath and the slag forms a deposit on the surface of the probe. The probe with the attached deposit is removed from the bath after a selected period of time and is rapidly cooled to preserve the deposit structure present at temperature. The molten bath was maintained at conditions corresponding to equilibrium with metallic copper. The deposit microstructure was then examined using a range of optical and scanning electron microscopy techniques as well as electron-probe X-ray microanalysis (EPMA) to accurately measure the compositions of the individual phases formed. The EPMA Superprobe JEOL-8200L (JEOL Ltd., Tokyo, Japan) was operated at 15 kV accelerating voltage and 15 nA probe current. The following standards were used for calibrations: Fe<sub>2</sub>O<sub>3</sub>, Al<sub>2</sub>O<sub>3</sub>, CaSiO<sub>3</sub> (from the Charles M. Taylor Co., Stanford, CA), and Cu<sub>2</sub>O (prepared in-house using Cu<sub>2</sub>O, 99.99 wt pct). The standard Duncumb-Philibert ZAF correction procedure supplied with the probe was used. The average accuracy of the EPMA measurements is estimated to be within 1 wt pct.

Measurements have been undertaken for a range of process conditions to determine the influence of process time on the deposits formed from the copper-containing silicate slag (see Table I). The synthetic slag used in the experiments was prepared from high-purity (99.9 wt pct) oxide powders; the bulk slag composition is constant during the experiments with different immersion times (see Table I) and very similar to part I of this series with the liquidus temperature of 1413 K (1140 °C) in equilibrium with metallic copper. The primary phase of delafossite, Cu<sub>2</sub>O.(Fe, Al)<sub>2</sub>O<sub>3</sub>, is experimentally determined in the supporting experiments.<sup>[10]</sup>

## III. RESULTS

### A. Effect of Immersion Time

A series of experiments was carried out for different immersion times to determine the steady-state conditions (see Table I for the bath compositions and process conditions). Figure 1(a) shows the change in temperature in the deposit and the surrounding liquid as a function of immersion time for a given set of process conditions. The temperatures measured by thin thermocouples were used to interpolate the thermal profile across the deposit (Figure 1(b)) as a function of thermocouples location using a one-dimensional (1-D) logarithmic heat-transfer equation.<sup>[10]</sup> An analysis of the microstructures (Figure 2) and temperature trends (Figure 1(a)) indicates that the deposit reached a steady-state thickness between 1 hours and 2.5 hours immersion time; the thickness of the deposit at 2.5 hours is equal to that at 9 hours (Figure 2(g)). Also, for the steady-state thickness, the apparent linear velocity at the surface of the deposit relative to the surrounding liquid was approximately estimated to be 0.05 ms<sup>-1</sup> (see Table I, the thickness of stagnant deposit was used for the calculation of linear velocity).

Figures 2 and 3 show the thicknesses of deposits at different immersion times and the microstructures in the deposits at steady-state conditions, respectively. Based on the analysis of previous<sup>[11–16]</sup> and present observations<sup>[10]</sup> of the microstructures in the deposits, the following classification is used to describe the different types of layers within the deposits (in order starting from the material immediately adjacent to the cold probe surface): 1) glassy layer, 2) glass-with-fine-microcrystalline layer, 3) closed crystalline layer, 4) open crystalline layer, and 5) residual bath materials, labeled 1 to 4 and 6 on the figures, and these are observed in all deposits examined in the current study.

### B. Phases in Freeze-Lining Deposit

Silicate glass or liquid, cuprite (Cu<sub>2</sub>O), delafossite Cu<sub>2</sub>O.(Fe, Al)<sub>2</sub>O<sub>3</sub>, and metallic copper were observed in all the freeze-lining deposits. The mean compositions of these phases at different distances from the cold surface

**Table I. Process Conditions and Bulk Slag Bath Compositions (Weight Percentage) for Different Immersion Times at Equilibrium with Metallic Copper**

Process Conditions	Composition of Bulk Slag Bath (wt pct) at Different Immersion Times					
	Immersion times	Al <sub>2</sub> O <sub>3</sub> pct	SiO <sub>2</sub> pct	Fe <sub>2</sub> O <sub>3</sub> pct	Cu <sub>2</sub> O pct	
Immersion times	1, 10, 30 min, 1, 2.5, 9 h					
		1 min	6.8	14.9	15.4	62.9
		10 min	6.5	15.1	15.7	62.7
		30 min	6.5	15.4	15.8	62.3
Air flow rate (l min <sup>-1</sup> )	100	1 h	7.3	15	14.8	62.9
Bath temperature, K (°C)	1438 (1165)	2.5 h	7.6	14.4	15.9	62.1
Speed of rotation (RPM)	20	9 hours	6.3	15.2	16.1	62.4
Estimated linear velocity of the deposit interface at steady-state (ms <sup>-1</sup> )*	0.05					

\*This is an estimated apparent linear velocity at the deposit surface calculated on the assumption that it is generated only by the rotation of the crucible and does not include other flow components, such as, natural convection and other.

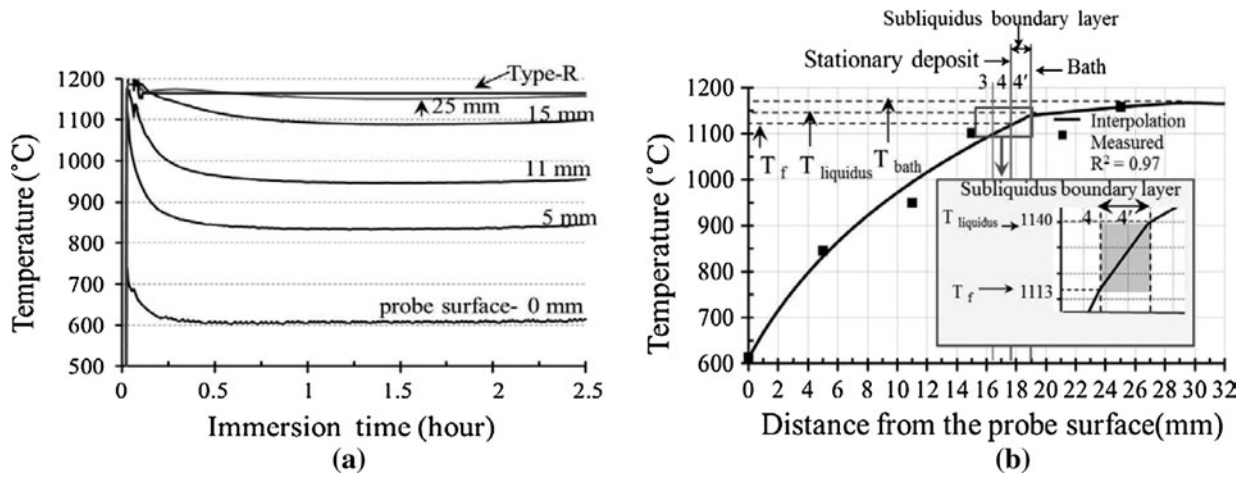


Fig. 1—(a) Temperature vs immersion time at positions across the freeze-lining deposit and bath. (b) Temperature distribution across the deposit and bath at steady-state conditions at bath temperature: 1438 K (1165 °C), air flow rate: 100 L min<sup>-1</sup> speed of rotation: 20 RPM (0.05 ms<sup>-1</sup>, for steady-state thickness), and immersion time: 2.5 h.

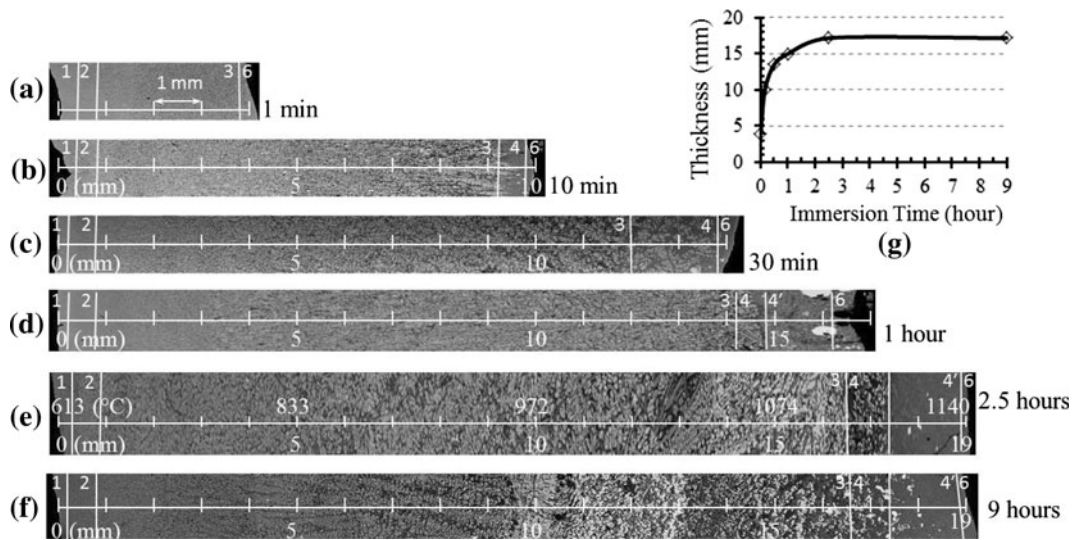


Fig. 2—Cross sections of freeze-lining samples obtained at bath temperature: 1438 K (1165 °C), air flow rate: 100 L min<sup>-1</sup>, speed of rotation: 20 RPM (0.05 ms<sup>-1</sup>, for steady-state thickness), and immersion times at (a) 1 min, (b) 10 min, (c) 30 min, (d) 1 h, (e) 2.5 h, and (f) 9 h. The probe and bath are located to the far left and right end of each of the SEM images, respectively.

of the probe for a given set of conditions are reported in Table II.

The initial thermodynamic calculations were undertaken using the FactSage program (ThermFact Inc., Montréal, Canada)<sup>[17]</sup> and recently developed thermodynamic database.<sup>[18]</sup> It indicates that the primary phase is delafossite at equilibrium with a liquidus temperature of 1423 K (1150 °C); at a lower temperature, the cuprite phase (Cu<sub>2</sub>O) is formed at approximately 1373 K (1100 °C), and tridymite is formed from the remaining liquid at 1348 K (1075 °C). The solidus is predicted to be at ~1338 K (1065 °C). Experimentally,<sup>[10]</sup> liquidus temperature has been shown to be 1413 K (1140 °C) and the eutectic temperature is below 1323 K (1050 °C) (Table II).

Cuprite mainly consists of copper (I) oxide (approximately 98 wt pct); the solubility of silica and alumina in

cuprite is almost zero, and the concentration of iron oxide dissolved in cuprite changes from 1.6 wt pct at 5 mm (~1106 K [833 °C]) to 0.5 wt pct at 16.5 mm (1373 K [1100 °C]), from cold finger (Table II).

Delafossite was present in all deposit layers, except the fully glassy layer (layer 1). In the presence of alumina in the bath, delafossite forms a solid solution with chemical formula of Cu<sub>2</sub>O.(Fe, Al)<sub>2</sub>O<sub>3</sub>. The concentration of Cu<sub>2</sub>O in delafossite does not change significantly, but Fe<sub>2</sub>O<sub>3</sub> changes from 25.1 wt pct close to the bath (corresponding to 1413 K [1140 °C] at 19 mm) to 45.8 wt pct close to the cold probe surface (at 2 mm from the probe corresponding to 989 K [716 °C]; see Table II).

Figure 4 shows the change in the concentration of iron (III) and alumina and the temperature profile at delafossite as a function of the distance from the cold-

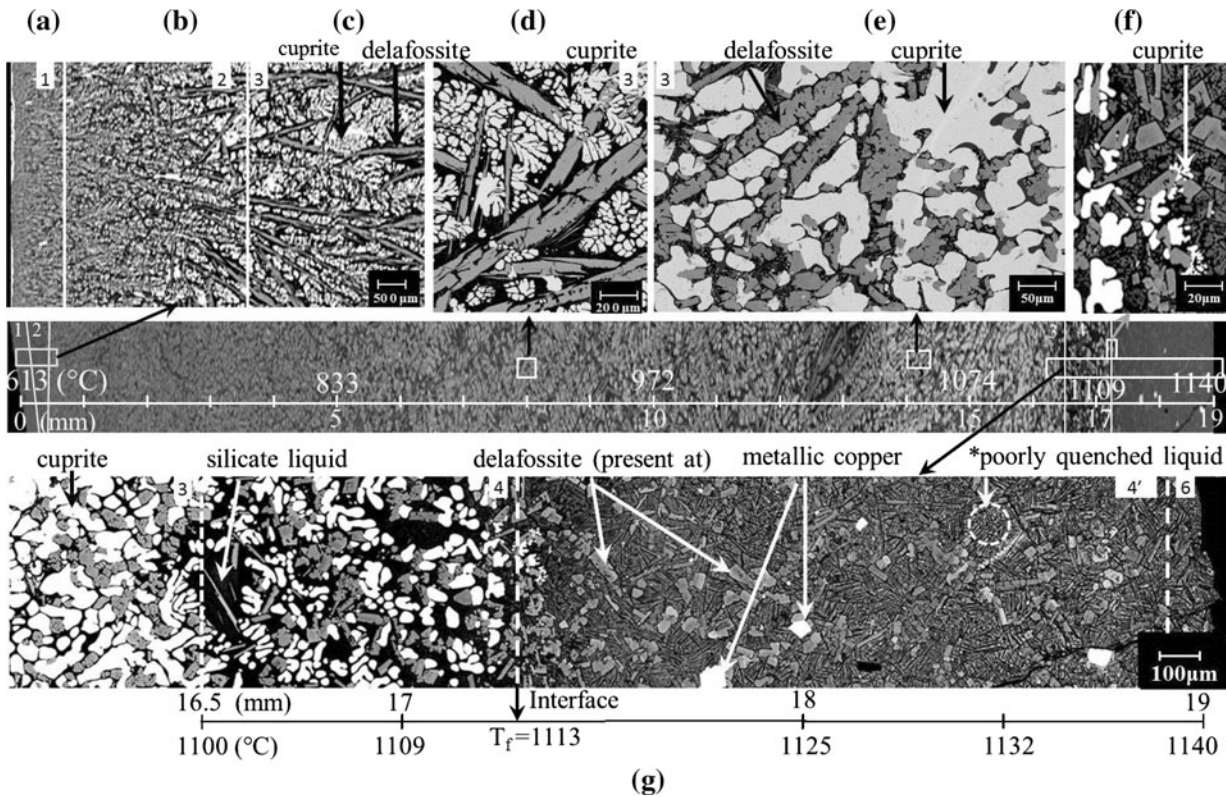


Fig. 3—Microstructures of freeze-lining sample at bath temperature: 1438 K (1165 °C), air flow rate: 100 L min<sup>-1</sup>, speed of rotation: 20 RPM (0.05 ms<sup>-1</sup>, for steady-state thickness), and immersion time 2.5 h. SEM micrographs of (a) glass layer (layer 1), (b) glass-with-fine-microcrystalline layer (layer 2), (c–e) closed crystalline layer (layer 3), (f–g) open crystalline layer (layer 4), and subliquidus boundary layer (layer 4'). \*‘‘Poorly’’ quenched liquid refers to material that was fully liquid at the high temperature, but it formed fine ‘‘quench crystals’’ on rapid cooling after the experiment. This area also contains larger crystals of delafossite that were present in the liquid at high temperature.

finger surface. The composition of delafossite remains almost constant from 2 mm (having approximately 989 K [716 °C]) to a distance of approximately 12 mm (~1289 K [1016 °C]) from the probe surface. At a further distance from the probe (>12 mm), the proportion of alumina in delafossite increases significantly and is close to the equilibrium composition (see the solid square in Figure 4). The difference from equilibrium compositions appears to increase in lower temperature locations at steady-state conditions. Also, the size and morphology of delafossite at 2.5 and 9 hours immersion time are very similar.

The composition of the silicate liquid/glass phase changes significantly with distance from the cold probe surface where the silica concentration decreases and the copper oxide concentration increases (Table II and Figures 5(a) and (b)). Precise identification of the transient between the closed crystalline layer (layer 3) and the open crystalline layer (layer 4) from two-dimensional (2-D) microstructure is not possible because some open channels might be available in three dimensions. However, Figure 3(e) suggests all liquid channels are blocked by high proportion of solids, in addition the presence of open crystalline layer (4) is obvious in freeze-lining microstructure and used as a criterion to delineate the boundary between closed (layer 3) and open (layer 4) crystalline layers (Figure 3(g)). Changes in phase compositions were also used to

support the identification of the boundary between the closed and open crystalline layers. Silica concentrations in the silicate glass/liquid are slightly higher than the equilibrium values (see the solid square in Figure 5(b) that indicates experimental values); this could be taken as an indication that the diffusion through the open channels has not been completed or local equilibrium was not achieved.

#### IV. DISCUSSION

An analysis of the microstructures revealed that noticeably absent from the deposits formed at steady-state conditions was a sealing primary phase layer between the stationary deposit and the bulk liquid. This observation was quite unexpected and one that was in clear contradiction to the previous understanding of the behavior of these systems, which assumed that at steady-state conditions the liquid must be in direct contact with a sealing primary phase material at the liquidus temperature. The ‘‘interface of the freeze-lining deposit and the bath’’ (or ‘‘hot face of the freeze lining deposit’’) is defined here as the boundary surface between agitated liquid layer of the bath and the stagnant, stationary layer of the freeze lining, the latter consisting of either entirely solid phase(s) or a combination of the liquid and

**Table II. Mean Compositions of Observed Phases Across the Freeze Lining at Bath Temperature: 1438 K (1165 °C), Air Flow Rate: 100 L Min<sup>-1</sup>, Speed of Rotation: 20 RPM (0.05 Ms<sup>-1</sup>), and Immersion Time 2.5 h**

Distance from the Cold Probe (mm)	Silicate glass or liquid (wt pct)					Delafossite (wt pct)					Cuprite (wt pct)					Original Temperature, K (°C)	Layer
	Al <sub>2</sub> O <sub>3</sub>	SiO <sub>2</sub>	Fe <sub>2</sub> O <sub>3</sub>	Cu <sub>2</sub> O	Original Total	Al <sub>2</sub> O <sub>3</sub>	SiO <sub>2</sub>	Fe <sub>2</sub> O <sub>3</sub>	Cu <sub>2</sub> O	Original Total	Al <sub>2</sub> O <sub>3</sub>	SiO <sub>2</sub>	Fe <sub>2</sub> O <sub>3</sub>	Cu <sub>2</sub> O	Original Total		
0 (glass)	6.8	15.5	14.5	63.2	99.3											886 (613)	1
1						3.4	0.2	45.8	50.6	99.7						941 (668)	1, 2, 3
2						3.7	0.1	45.7	50.5	99.5						989 (716)	3
3						3.7	0.1	45.6	50.6	99.3						1032 (759)	
4	13.2	61.5	5.0	20.3	98.7	3.6	0.1	45.8	50.5	99.3	0.0	0.1	1.6	98.3	100.4	1071 (798)	
5	13.3	61.5	4.5	20.7	99.3	3.7	0.1	45.7	50.5	99.2	0.0	0.0	1.5	98.5	99.0	1106 (833)	
6	13.2	63.1	3.8	19.9	99.3	3.7	0.1	45.7	50.5	99.2	0.0	0.0	1.5	98.5	100.0	1138 (865)	
7	13.2	63.2	3.8	19.8	99.3	3.8	0.1	45.6	50.5	99.3	0.0	0.0	1.5	98.5	100.0	1368 (895)	
8	13.2	63.1	3.8	19.9	99.1	3.8	0.1	45.6	50.5	99.3	0.0	0.0	1.3	98.7	100.1	1195 (922)	
9	13.1	63.2	3.9	19.8	99.0	3.9	0.1	45.4	50.6	99.3	0.0	0.0	1.5	98.5	100.2	1221 (948)	
10	13.0	63.0	4.0	20.0	99.0	3.9	0.1	45.4	50.6	99.3	0.0	0.0	1.5	98.5	100.1	1245 (972)	
11	12.8	62.7	4.2	20.3	98.9	3.9	0.1	45.5	50.5	99.3	0.0	0.0	1.4	98.6	100.9	1268 (995)	
12	11.1	58.5	5.4	25.0	97.6	5.1	0.0	44.5	50.4	99.2	0.0	0.0	1.2	98.8	99.7	1289 (1016)	
13	10.6	56.7	5.9	26.8	96.2	8.5	0.0	39.9	51.6	100.4	0.0	0.0	1.1	98.9	100.6	1310 (1037)	
equilibrium*	12.2	49.4	7.3	31.1	100.4	13.7	0.1	36.5	49.7	101.4	0.0	0.1	0.8	99.1	99.9	1323 (1050)	
14	10.3	53.0	7.1	29.6	101.3	10.0	0.1	39.7	50.2	99.7	0.0	0.0	0.9	99.1	100.4	1329 (1056)	
15	10.1	51.4	7.6	30.9	100.6	11.5	0.0	36.9	51.6	99.8	0.0	0.0	0.7	99.3	100.2	1347 (1074)	
16	9.4	46.6	8.5	35.5	101.5	13.5	0.1	33.3	53.1	99.5	0.0	0.0	0.5	99.5	100.8	1365 (1092)	
16.5	10.8	43.9	9.6	35.7	100.6	14.7	0.1	32.2	53.0	100.8	0.0	0.0	0.5	99.5	100.1	1373 (1100)	
Equilibrium*	12.0	37.6	8.0	42.4	101.1	16.2	0.1	33.6	50.1	100.6	0.0	0.2	0.2	99.6	100.2	1373 (1100)	4
17	9.9	38.2	11.4	40.5	99.9	16.0	0.0	31.0	53.0	100.5	0.0	0.0	0.2	99.6	100.2	1382 (1109)	
17.5	7.6	26.9	11.6	53.9	98.9	16.2	0.0	31.0	52.8	100.2	0.0	0.0	0.2	99.6	100.2	1390 (1117)	
18	6.9	23.1	13.2	56.8	99.3	16.8	0.1	30.2	52.9	100.5	0.0	0.0	0.2	99.6	100.5	1398 (1125)	4'
18.5	6.5	20.3	12.2	61.0	99.6	18.2	0.1	28.6	53.1	100.9	0.0	0.0	0.2	99.6	100.9	1405 (1132)	
19	7.3	16.7	13.2	62.8	100.1	20.5	0.1	25.1	54.3	100.7	0.0	0.0	0.2	99.6	100.7	1413 (1140)	
Equilibrium*	6.9	15.5	15.7	61.9	100.8	24.1	0	22.5	53.4	101.3	0.0	0.0	0.2	99.6	100.8	1413 (1140)	
Bath before	7.6	14.4	15.9	62.1	99.5											1438 (1165)	
Bath after	7.5	15.0	15.6	61.9	100.8											1438 (1165)	

\*Results of experiments in equilibrium with metallic copper from part I of this study.<sup>[10]</sup>

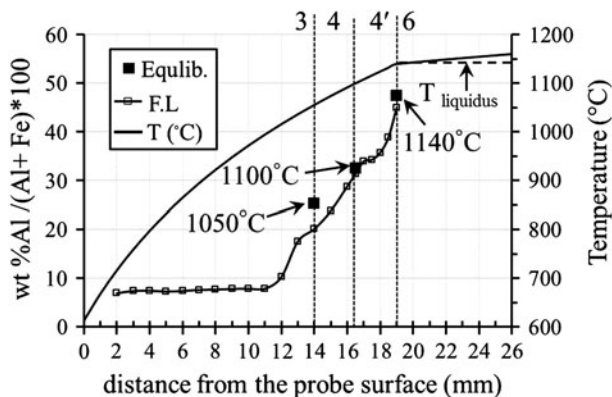


Fig. 4—Composition of delafossite as a function of distance from the probe surface and temperature for freeze-lining and equilibrium experiments at bath temperature: 1438 K (1165 °C), air flow rate: 100 L min<sup>-1</sup>, speed of rotation: 20 RPM (0.05 ms<sup>-1</sup>, for steady-state thickness), and immersion time 2.5 h (F.L and equilb. refer to freeze-lining and equilibrium experiments, respectively).

solid phases, where solid phases cannot be “washed” away into the liquid bath.

For example, as can be seen from the microstructures given in Figure 6, the interface between the stagnant deposit and liquid bath consists of three phases, delafossite, cuprite, and a silica-enriched liquid phase. This is a clear indication that the deposit–bath interface temperature ( $T_i$ ) is lower than the liquidus of the bulk liquid ( $T_{\text{liquidus}}$ ). The question is why does the freeze-lining not continue to grow until a solid layer of primary phase crystals forms, the bath/deposit interface reaches the liquidus temperature, and chemical and thermal equilibrium with the bulk liquid is established? The presence of delafossite at the deposit interface indicates that there is no nucleation barrier to the crystallization of the primary phase on the existing solid phase surfaces.

A careful, systematic analysis of the deposit microstructures and phases from different samples (at this paper and part I<sup>[10]</sup>) indicates that, at steady-state conditions, the interface of the stationary deposit is at subliquidus temperatures. The evidence of that is presence of cuprite at the interface between the freeze lining deposit and the liquid layers (see, for example, Figures 3(f) and 6(a) where cuprite from the freeze lining is in direct physical contact with the liquid). Note that the specifically focused experimental study reported in part I<sup>[10]</sup> has confirmed that the primary phase for this bulk bath slag composition is be delafossite, and that cuprite starts to precipitate at temperatures that are below the liquidus temperature.

Another clue to this behavior can be found by examining the liquid bath layer immediately adjacent to the stationary deposit (Figure 6(a)). This represents the boundary layer between the bulk liquid and the deposit, at which there is continuous heat transfer from the outer layer through the stationary deposit to the cold probe, and intensive diffusive and convective mass transfer of the “fresh chemicals” is expected from the bulk bath to the interface through the intensively

agitated liquid layers. When the cold finger is removed from the bath, some material from the bulk liquid adjacent to the deposit is also removed and quenched when the deposit is rapidly cooled. An examination of this quenched “bath material” reveals that, in addition to the fine cuprite and delafossite “quench crystals” in a matrix of residual silicate glass that formed on rapid cooling after the experiment, there are relatively large, 10–50  $\mu\text{m}$ , primary phase delafossite crystals. The relatively large size and the morphology indicate these crystals had been present at a temperature in the melt prior to quenching. Primary phase delafossite crystals up to 50  $\mu\text{m}$  in diameter are also found in the bulk liquid bath material (Figure 6(c) shows the microstructure of a bath sample taken 50 mm away from the deposit interface). The presence of primary phase delafossite crystals ahead of the deposit interface is apparent in the sample illustrated in Figure 7, approaching steady-state conditions. In addition, EPMA measurements show that there is a significant change in liquid composition across the “subliquidus boundary layer” between the steady-state deposit interface and the bulk bath liquid (Figures 5(a) and (b) and shown schematically in Figure 6(b)); in particular, the silica concentration in the liquid phase increases and the copper and iron concentrations correspondingly decrease as the deposit interface is approached from the liquid bath (Figures 5(a) and (b)).

It appears that the steady-state conditions represent a state of dynamic equilibrium that is critically dependent on the relative rates of crystallization, mass transfer processes, and heat transfer processes occurring close to and at the deposit interface. Conceptually, this mechanism is quite different from the previously accepted assumption of the thermal and chemical equilibrium at the interface at liquidus conditions.

The proposed mechanism is explained with the introduction of the concept of a “subliquidus boundary layer” (layer 4') as follows. As the result of the natural and forced convection (the latter induced by the rotating crucible), fresh portions of liquid move from the bulk bath toward the stationary deposit with the temperature decreasing from the bath temperature  $T_{\text{bath}}$  to the liquidus temperature  $T_{\text{liquidus}}$  without crystallization (Figures 6(b) and (c)). As the liquid portion crosses the point with  $T_{\text{liquidus}}$  and its temperature decreases below  $T_{\text{liquidus}}$ , nucleation and precipitation of the primary phase delafossite (crystallizing delafossite) (and later cuprite) starts (Figure 6(c)). As a result, the composition of the remaining liquid also changes. If the movement of the portion of liquid with the primary phase crystals toward the interface is slow compared to the crystallization rate, then the local equilibrium between the primary delafossite and cuprite crystals and the surrounding liquid is maintained during this passage across the “subliquidus boundary layer (layer 4'”) through short-range diffusion within this portion of liquid. The copper-containing slags used in the current study contain significant concentrations of silica; on removal of the iron and copper components from the liquid phase through the delafossite precipitation, the silica concentration in the remaining liquid, and there-

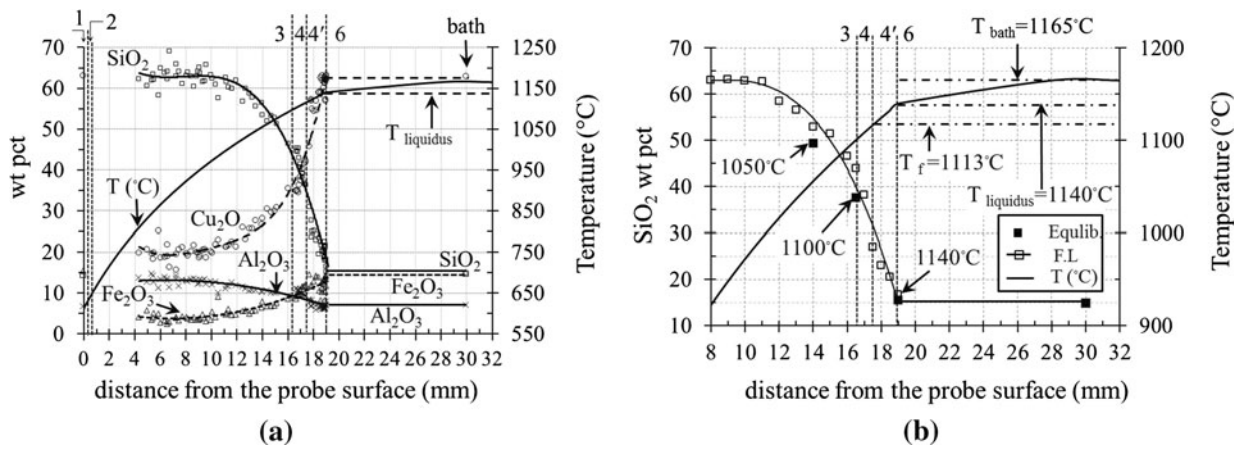


Fig. 5—Composition of silicate glass/liquid (a) as a function of distance from the probe surface, (b) detailed of deposit–liquid interface at bath temperature: 1438 K (1165 °C), air flow rate: 100 L min<sup>-1</sup>, speed of rotation: 20 RPM (0.05 ms<sup>-1</sup>, for steady-state thickness), and immersion time: 2.5 h (composition lines show just a trend line). F.L and equilb. refer to freeze-lining and equilibrium experiments, respectively.

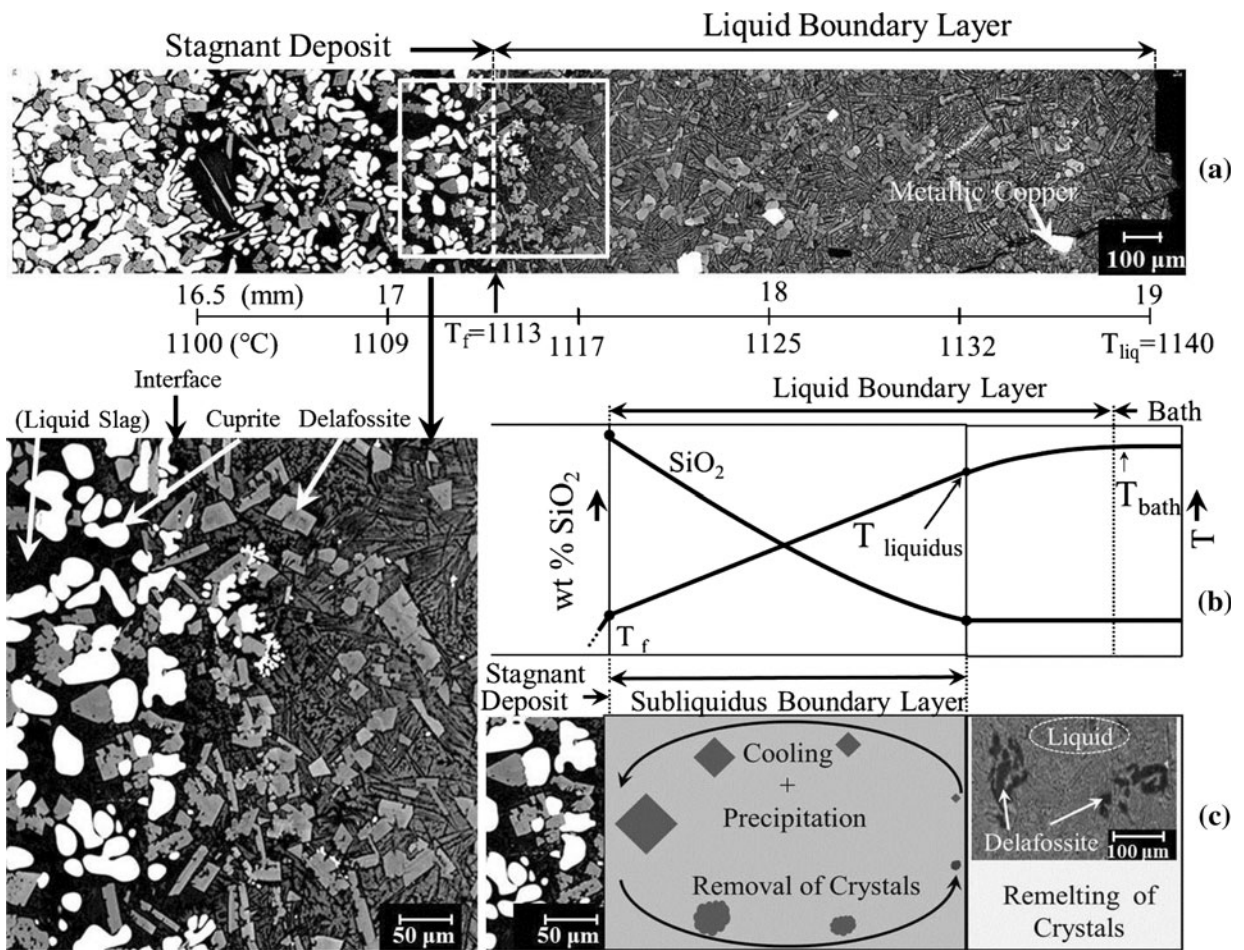


Fig. 6—A cross section of freeze-lining sample illustrating the stagnant and subliquidus boundary layers. Bath temperature: 1438 K (1165 °C), air flow rate: 100 L min<sup>-1</sup>, speed of rotation: 20 RPM (0.05 ms<sup>-1</sup>, for steady-state thickness), and immersion time: 2.5 h. (a) Deposit liquid interface, (b) schematic of assumed boundary layers, and (c) proposed mechanisms taking place within the boundary layer at steady-state conditions.

fore the liquid viscosity, will both increase thus slowing the convective flow. If the rate of crystallization is fast compared to the rate of transport of the liquid portion with the crystals across the subliquidus boundary layer,

then the liquid phase arrives at the deposit interface with no thermodynamic driving force to form further delafossite at the main stationary deposit interface either as fresh precipitates on existing crystals or by cementing

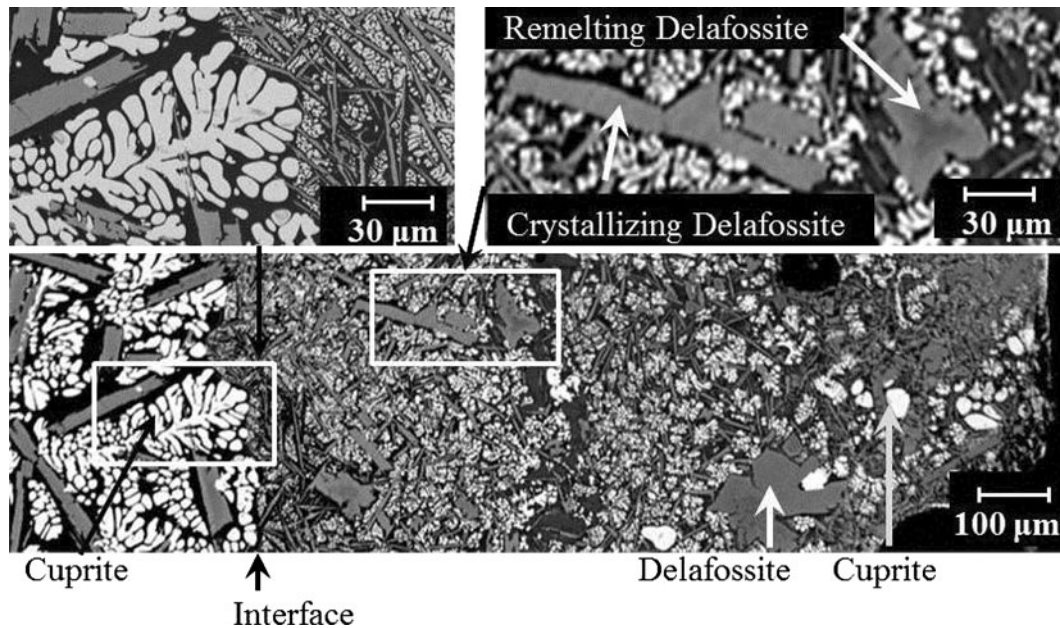


Fig. 7—Microstructure of the deposit–bath interface. Slag composition, 6.5 wt pct  $\text{Al}_2\text{O}_3$ , 15.4 wt pct  $\text{SiO}_2$ , 15.8 wt pct  $\text{Fe}_2\text{O}_3$ , 62.3 wt pct  $\text{Cu}_2\text{O}$ ; bath temperature, 1438 K (1165 °C), air flow rate:  $100 \text{ L min}^{-1}$ , speed of rotation: 20 RPM ( $0.05 \text{ ms}^{-1}$ , for steady-state thickness), and immersion time 1 h.

the precipitated delafossite crystals from the liquid to the deposit. The delafossite crystals arriving through the subliquidus boundary layer therefore do not become attached to the deposit surface. It is well established<sup>[19]</sup> that mass transfer at interfaces occurs through the formation of flow cells or turbulent eddies enabling the simultaneous flow to and from the interface, so that the forced and natural convective flow of the liquid not only brings crystals to the deposit interface but also transports portions of liquid with the precipitated crystals away from the deposit interface back into the bulk liquid. The precipitated crystals will redissolve into the bulk liquid (remelting delafossite) as they will be washed away into the regions where the temperature is above the liquidus.

Additional evidence supporting the proposed mechanism is a presence of the cuprite crystals precipitated on the delafossite grains freely floating in the subliquidus boundary layer 4' (Figures 3(f) and 6)—these cuprite crystals appear to be formed while this portion of the layer 4' was moving toward the interface.

The proposed mechanism, involving the development of the subliquidus boundary layer (layer 4'), is not only consistent with the flow cell concept but also explains how newly formed crystals of delafossite (crystallizing delafossite) in the melt can be brought close to the deposit interface and then can subsequently be moved away without attachment, as well as how these crystals can be partially or fully remelted (remelting delafossite) as they are transferred back to the areas with higher temperatures that exist in the bulk bath (Figure 6(c)).

This mechanism suggests that the formation of different types of the interface between the stagnant freeze-lining deposit and the liquid bath, the formation of the subliquidus boundary layer (layer 4'), and the

absence or presence of the primary-phase sealing layer (layer 5) are determined by the combination of the slag properties (*i.e.*, viscosity, mass diffusivity, nucleation, crystallization, dissolution kinetics, and liquidus shape of phase equilibrium) and the convective flow pattern of the liquid bath.

#### A. Classification of Freeze Lining (Types of Deposit)

The fact that the bath–deposit interface temperature ( $T_f$ ) may be lower than the liquidus ( $T_{\text{liquidus}}$ ) (described above) can be taken as the basis for the assumption that the stabilization mechanisms of freeze linings with different interface temperatures would be significantly different, and these mechanisms in turn determine all of the main stagnant freeze-lining deposit characteristics, such as thickness, stability, heat transfer, and other properties. A new classification of freeze linings is proposed based on the comparison between the steady-state stagnant interface temperatures to facilitate further analysis of the factors controlling freeze lining.

##### 1. Interface temperature greater than the liquidus temperature of the bulk liquid ( $T_f > T_{\text{liquidus}}$ )

This type of deposit is a usual case with refractory lining and is included here for completeness of the classification. The deposit may form on the hot face of the refractory with some mass transfer (*e.g.*, by diffusion) of the high-melting components from the refractory material (*e.g.*,  $\text{MgO}$  and  $\text{Cr}_2\text{O}_3$ ) through the stagnant part of the freeze lining to the interface with the liquid bath. This can lead to formation of the solid phases at the interface having higher concentrations of “refractory” elements and thus made more stable compared to the equilibrium primary phase of the bath



materials. Therefore, the interface temperature between this stagnant layer and the liquid may be higher than the liquidus of the bulk bath. The continuous mass transfer from the refractory to the freeze-lining interface, followed up by continuous slow dissolution of the freeze-lining material into the bath as well as possible erosion of particles from the freeze-lining into the liquid bath, may continuously consume the refractory. However, this process may be slow and might guarantee furnace integrity for extended periods of time.

2. *Interface temperature equal to the liquidus temperature of the bulk liquid ( $T_f = T_{\text{liquidus}}$ )*

Relatively fast mass transfer from the liquid to the freeze-lining interface can result in the crystallization of the primary phase crystals forming a stable primary-phase-sealing layer (layer 5) with the temperature of the interface between the freeze lining and the liquid bath at steady-state conditions equal to the liquidus temperature of the bulk liquid bath. Under the proposed mechanism, the fast mass transfer from the liquid bath to the freeze-lining interface is essential for the formation of this type of deposit. It is to be expected that these high mass transfer rates would be achieved in the systems having relatively fluid liquids or for the intensive bath convection conditions.

3. *Interface temperature between the bulk bath liquidus and glass transition temperature ( $T_g < T_f < T_{\text{liquidus}}$ )*

As described in Section IV, a subliquidus boundary layer (layer 4') between the stagnant deposit (crystalline open layer [layer 4] or crystalline closed layer [layer 3]) and the liquid bath with the temperature gradient between the bath liquidus temperature and the interface temperature may form. Consequently, crystallization takes place in the subliquidus boundary layer as material moves from the bulk of the bath and cools at the same time, so that when it reaches the interface, the remaining liquid (after crystallization) is in equilibrium with the solids and there is no driving force for further crystallization. As the liquid and solids material is moved by convection back toward the bulk of the bath, it reheats, and the solids are dissolved back into the liquid. The formation of subliquidus boundary layer with continuous crystallization on the way toward the interface with the stagnant layer and redissolution on the way from the interface is believed to result in the temperature of the interface  $T_f$  being lower than the liquidus of the bulk bath  $T_{\text{liquidus}}$ . This type of the deposit is expected in the systems with relatively low mass transfer rates (both convective and diffusive) that is characteristic of the liquids with higher viscosities and of the relatively less agitated baths, thus allowing the crystallization to be completed as the material moves toward the interface and cools. The interface layer of the stagnant part of the deposit may be open (layer 4) or closed (layer 3) for mass exchange with the liquid bath.

4. *Interface temperature lower than glass transition temperature ( $T_f < T_g$ )*

It may be concluded that the systems with high glass transition temperatures and slow crystallization kinetics

may have the freeze-lining deposit with the interface temperature lower than the glass transition temperature. The interface layer of the stagnant part of the freeze-lining deposit in this case would be the glass or the microcrystalline type.

## B. *Verification of Proposed Mechanism of the Freeze-Lining Stabilization*

Having developed a new conceptual model that explains the mechanism of stabilization of subliquidus deposit-liquid interfaces at steady-state conditions, a careful reevaluation of the factors determining formation and stability of the stationary steady-state deposits has been undertaken. The proposed mechanism suggests that different types of interface structure between the stagnant freeze-lining deposit and the liquid bath may be formed and that the absence or presence of the primary-phase sealing layer at steady state is determined not only by chemical equilibrium alone but also by the combination of the system parameters, including slag properties (such as viscosity, thermal and mass diffusivity, nucleation and crystallization kinetics, liquidus shape of phase equilibrium, and dissolution kinetics) as well as the convective flow patterns within the liquid bath.

The proposed mechanism was then tested experimentally in the following way. If the proposed mechanism is correct, then it is expected that the interface type and temperature may be changed by the changing properties of the system by changing bulk chemistry of bath agitation. For example, it is expected that the primary phase sealing layer with the bath-deposit interface temperature equal to  $T_{\text{liquidus}}$  of the bulk bath would form if the mass transfer across the boundary layer toward the interface is faster than crystallization—this condition is anticipated in low viscosity melts. To test this concept, an experiment was undertaken with a bulk liquid composition having a lower silica concentration (5.2 wt pct  $\text{Al}_2\text{O}_3$ , 9.2 wt pct  $\text{SiO}_2$ , 9.6 wt pct  $\text{Fe}_2\text{O}_3$ , and 76.0 wt pct  $\text{Cu}_2\text{O}$ ) than in the original slag and, therefore, one having lower viscosity. The detailed temperature measurements show that under these conditions, the freeze lining reached a steady-state thickness after the shorter time of approximately 1 hour. The microstructure of the deposit cross section shown in Figure 8 demonstrates clearly that a dense primary phase sealing layer of delafossite (layer 5) is formed at the deposit–bath interface; under this condition, the interface temperature must therefore be that of the bulk bath liquidus temperature,  $T_{\text{liquidus}}$ .

The hypothesis was further experimentally tested in a very different chemical system involving the use of a molten fluoride salt bath, which is well known to have very low viscosities. Figure 9 shows an example of a deposit produced from a molten salt bath with the columnar growth and dense sealing layer of primary phase cryolite,  $\text{Na}_3\text{AlF}_6$ , crystals at the deposit/melt interface in this system. This is a further evidence to support the proposed mechanism and the argument that the mass transfer characteristics at the interface and physicochemical properties of the melt can influence product structure and the thermal conditions present at the interface.

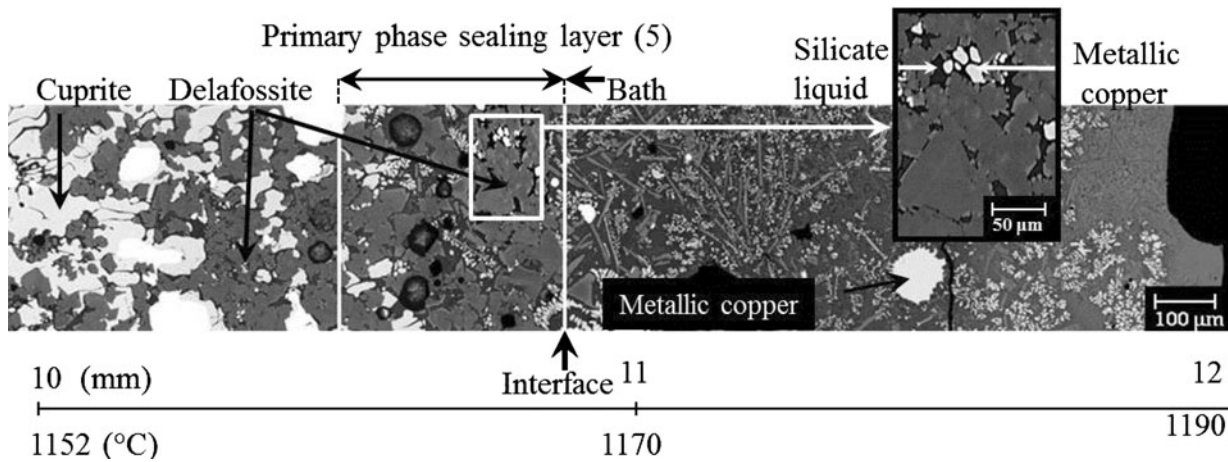


Fig. 8—Cross section of steady-state freeze-lining illustrating the formation of a dense, primary phase sealing layer of delafossite at the deposit/bath interface. Bulk liquid composition, 5.2 wt pct  $\text{Al}_2\text{O}_3$ , 9.2 wt pct  $\text{SiO}_2$ , 9.6 wt pct  $\text{Fe}_2\text{O}_3$ , and 76.0 wt pct  $\text{Cu}_2\text{O}$ ; bath temperature, 1463 K (1190 °C); air flow rate, 100  $\text{L min}^{-1}$ ; speed of rotation, 20 RPM (0.04  $\text{ms}^{-1}$ , for steady-state thickness); and immersion time 2.5 h.

## V. IMPLICATIONS FOR INDUSTRIAL PRACTICE

To date, the approaches to freeze-lining design that have been used for industrial applications have been based solely on heat transfer considerations with assumption of the freeze-lining interface to have the liquidus temperature of the bulk bath slag. Thermal parameters, such as bath convection, superheat, and the heat-removing capacity of the coolant from the interface of the deposit and bath, were believed to be the main parameters determining the thickness of the freeze lining at steady-state conditions. An important assumption in all of these previous models has been that the liquidus temperature defines the interface between the stable freeze-lining deposit and the molten bath.<sup>[1-9]</sup>

From the review and analysis of the microstructures in the slag deposits obtained in the present and previous studies<sup>[10-16]</sup> it is clear that a range of different deposit morphologies can be developed during the formation of the deposit. The reasoning behind that assumption is that at steady-state conditions, the crystal phases are already present at the stationary deposit so there is no nucleation barrier to overcome. The attachment of atoms onto the existing crystals from the melts occurs readily, as facilitated by the heat removal from the interface through the freeze-lining deposit and by the mass transfer of the “fresh” chemicals from the bulk bath area. Because at steady state there is no net growth of the stationary deposit, there must therefore be no net thermodynamic driving force for crystal growth at this boundary, and this points the condition where the solid primary phase at the interface is in chemical and thermal equilibrium with the bulk liquid at the liquidus temperature.

### A. Layer 1: The Glassy Layer

In contact with and close to the cold finger is a layer of homogeneous glass. This is the first phase formed on contact of the probe with the melt, and as such, it experiences a high initial cooling rate. The composition

of the material is uniform and is identical to that of the bulk liquid. Because the material remains in contact with the probe throughout the experiment, it is retained below the glass transition temperature.

### B. Layer 2: Glass with Microcrystals

Immediately adjacent to the fully glassy layer is material that consists of a matrix of glassy or highly viscous liquid and varying proportions of fine precipitated crystalline solids. This layer appears to have formed initially as a glass or highly viscous liquid; the fine crystalline phases precipitated at some later time as the overall frozen deposit thickness increased. The bulk composition of this layer is the same as the bulk bath composition. In the current study, the fine precipitates are delafossite and cuprite crystals.

### C. Layer 3: The Closed Crystalline Layer

The material in this layer consists of predominantly crystalline solids; residual liquid is present between the crystalline structures. The crystals in this next layer appear to have precipitated directly from the liquid phase, originally above the glass transition temperature. The extent of crystallization in this layer is such that effectively there is no exchange of material with the bulk liquid bath. This layer in the freeze-lining in the present study contains large (greater than 100  $\mu\text{m}$ ) faceted delafossite precipitates and large dendritic cuprite crystals; the residual high-silica liquid occupies the intercrystalline regions. The bulk composition of this layer is the same as the bulk bath composition. The crystal dimensions increase with increasing distance from the cold probe.

### D. Layer 4: The Open Crystalline Layer

The next layer of the deposit consists of widely spaced, relatively large crystals with a significant liquid phase fraction and open liquid channels facilitating the relatively intensive convective and diffusive mass trans-

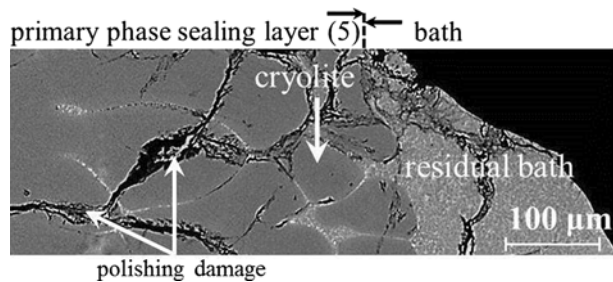


Fig. 9—SEM backscattered micrograph of the cross-section of freeze-lining sample obtained from molten salt showing the formation of dense columnar primary phase crystals of cryolite solid solution. Bath composition, 51.8 wt pct NaF, 8.7 wt pct  $\text{CaF}_2$ , and 39.5 wt pct  $\text{AlF}_3$ ; bath temperature, 1248 K (975 °C); air flow rate, 50  $\text{L min}^{-1}$ ; speed of rotation: 20 RPM ( $0.03 \text{ ms}^{-1}$ , for steady-state thickness); and immersion time 1.5 h. The sample was quenched in liquid nitrogen. The cold probe is located to the far left and the hot bath to the right of the figure.

fer from the bulk liquid bath. EPMA measurements have shown that the liquid composition in this layer varies significantly with distance from the deposit interface. This layer in the freeze lining investigated in the current study consists of the primary delafossite crystals, cuprite, and the silicate liquid.

#### E. Layer 4': Subliquidus Boundary Layer

The temperature is below the liquidus of the bulk bath in this layer, implying the potential for phase precipitation. This layer is an intermediate layer between stagnant deposit and liquid bath.

#### F. Layer 5: The Sealing Primary Phase

Theoretically at thermal steady-state and chemical equilibrium conditions, the deposit material in direct contact with the liquid bath should consist entirely of the primary phase crystals; it might reasonably be expected that a continuous dense sealing layer of the primary phase would be present under all conditions. This sealing primary phase layer was not observed in the steady-state deposits obtained in the current study.

In metal alloy<sup>[20–22]</sup> and sea ice<sup>[23]</sup> systems, dendrite arm remelting and detachment has been shown to occur and to be responsible for the transport of existing primary phase crystals into the bulk liquid. Although the dendrite remelting and fragmentation mechanisms occur under dynamic growth conditions rather than steady-state or stationary interfaces, they do, however, serve to demonstrate that local crystal growth and mass transport processes can have significant influences on interface development and structure, and that liquid microflow phenomena can be active in these systems.

## VI. CONCLUSIONS

It has been shown in the current study that the phase assemblage formed at the stationary deposit interface with the liquid bath at steady-state conditions is not

necessarily solely that of the primary phase. The observations indicate that the temperature of the steady-state deposit interface with the liquid bath can be lower than the equilibrium liquidus temperature of the bulk liquid. This is contrary to the previous understanding of the behavior in these systems.

A mechanism has been proposed that explains this unexpected phenomenon; this involves convective mass transfer and crystallization processes taking place in a liquid boundary layer immediately adjacent to the stationary-deposit interface identified as “subliquidus boundary layer.” The results of the supporting experiments in low-viscosity systems are consistent with the proposed mechanism. Importantly, the results indicate that a number of other system properties, including liquid properties (e.g., viscosity, thermal and mass diffusivity, nucleation and crystallization kinetics, liquidus shape of phase equilibrium and dissolution kinetics), fluid flow characteristics, and mass transfer rates close to and at the stationary deposit interface, are additional key parameters that must be included in design considerations; this represents a significant change in design philosophy and approach. Deposit formation should be regarded as a dynamic process that involves reactions in liquid boundary layer adjacent to the freeze-lining deposit. This then opens up opportunities for significant improvements in process performance and a deeper understanding of the fundamental mechanisms of deposit formation. It indicates the possibility of selecting process conditions below the liquidus temperature of the bulk bath that could result in significant energy savings and increases in the throughputs of the reactors.

A generic classification of freeze linings has been proposed, linking the interface temperatures to deposit microstructures at steady-state conditions. Although the focus of the current study has been on molten oxides (slags) and molten salt, the results can be applied to any chemical system having analogous boundary conditions.

## ACKNOWLEDGMENTS

The authors would like to thank the Australian Research Council Linkage program, Rio Tinto Kennecott Utah Copper, Corp., Xstrata Technology, Xstrata Copper, BHP Billiton Olympic Dam Operation, and Outotec Finland Oy for their financial support.

## REFERENCES

1. F. Guevara and G. Irons: *Metall. Mater. Trans. B*, 2011, vol. 42B, pp. 652–63.
2. F. Guevara and G. Irons: *Metall. Mater. Trans. B*, 2011, vol. 42B, pp. 664–76.
3. P.C. Pistorius: *SAIMM*, 2003, vol. 103 (8), pp. 509–14.
4. P.C. Pistorius: *SAIMM*, 2004, vol. 104 (7), pp. 417–22.
5. J.H. Zietsman and C. Pistorius: *Miner. Eng.*, 2005, vol. 19 (3), pp. 262–79.
6. D.G.C. Robertson and S. Kang: *Fluid Flow Phenomena in Minerals Processing*, TMS, Warrendale, PA, 1999, pp. 157–68.
7. K. Verscheure, M.V. Camp, B. Blanpain, P. Wollants, P. Hayes, and E. Jak: *Metall. Mater. Trans. B*, 2007, vol. 38B, pp. 13–20.

8. K. Verscheure, F. Verhaeghe, E. Boydens, M.V. Camp, B. Blanpain, and P. Wollants: *Metall. Mater. Trans. B*, 2006, vol. 37B, pp. 929–40.
9. K. Verscheure, A.K. Kylo, A. Filzwieser, B. Blanpain, and P. Wollants: *Proc. Conf. on Non-Ferrous Materials Extraction and Processing*, TMS, Warrendale, PA, 2006, pp. 139–54.
10. A. Fallah-Mehrjardi, P.C. Hayes, and E. Jak: *Metall. Mater. Trans. B*, 2013. doi:[10.1007/s11663-013-9806-z](https://doi.org/10.1007/s11663-013-9806-z).
11. M. Campforts, B. Blanpain, and P. Wollants: *Metall. Mater. Trans. B*, 2009, vol. 40B, pp. 643–55.
12. M. Campforts, E. Jak, B. Blanpain, and P. Wollants: *Metall. Mater. Trans. B*, 2009, vol. 40B, pp. 619–31.
13. M. Campforts, E. Jak, B. Blanpain, and P. Wollants: *Metall. Mater. Trans. B*, 2009, vol. 40B, pp. 632–42.
14. M. Campforts, K. Verscheure, E. Boydens, T.V. Rompaey, B. Blanpain, and P. Wollants: *Metall. Mater. Trans. B*, 2008, vol. 39B, pp. 408–17.
15. M. Campforts, K. Verscheure, T.V. Rompaey, E. Boydens, B. Blanpain, and P. Wollants: *Metall. Mater. Trans. B*, 2007, vol. 38B, pp. 841–51.
16. MiekeCampforts, K. Verscheure, F. Verhaeghe, T.V. Rompaey, E. Boydens, B. Blanpain, and P. Wollants: *Non-Ferrous Materials Extraction and Processing*, TMS, Warrendale, PA, 2006, pp. 309–21.
17. FactSage ver. 6.2., CRCT-Thermfact Inc & GTT-Technologies, Montreal, Canada, 2010.
18. T. Hidayat and E. Jak: *CALPHAD XLI* (private communication), Berkeley, CA, June 3–8, 2012.
19. P.V. Danckwerts: *Ind. Eng. Chem.*, 1951, vol. 43, p. 1460.
20. M.C. Flemings: *Solidification Processing*, McGraw-Hill, New York, NY, 1974.
21. W. Kurz and D.J. Fisher: *Fundamentals of Solidification*, 3rd ed., Trans Tech Publications, Aedermannsdorf, Switzerland, 1989.
22. D. Ruvalcaba, R.H. Mathiesen, D.G. Eskin, L. Arnberg, and L. Katgerman: *Acta Mater.*, 2007, vol. 55 (13), pp. 4287–92.
23. D.N. Thomas and G.S. Dieckmann: *Sea Ice: An Introduction to its Physics, Chemistry, Biology, and Geology*, Blackwell Science, New York, NY, 2003.